Photothermally Reduced Graphene as High-Power Anodes for Lithium-Ion Batteries

Rahul Mukherjee,[†] Abhay Varghese Thomas,[†] Ajay Krishnamurthy,[†] and Nikhil Koratkar[†,‡,*]

[†]Department of Mechanical, Aerospace and Nuclear Engineering and [‡]Department of Materials Science and Engineering, Rensselaer Polytechnic Institute, Troy, New York 12180, United States

ABSTRACT Conventional graphitic anodes in lithium-ion batteries cannot provide high-power densities due to slow diffusivity of lithium ions in the bulk electrode material. Here we report photoflash and laser-reduced free-standing graphene paper as high-rate capable anodes for lithium-ion batteries. Photothermal reduction of graphene oxide yields an expanded structure with micrometer-scale pores, cracks, and intersheet voids. This open-pore structure enables access to the underlying sheets of graphene for lithium ions and facilitates efficient intercalation kinetics even at ultrafast charge/discharge rates of >100 C. Importantly, photothermally reduced graphene anodes are structurally robust and display outstanding stability and cycling ability. At charge/discharge rates of ~40 C, photoreduced graphene anodes delivered a steady capacity of ~156 mAh/g_{anode} continuously over 1000 charge/discharge cycles, providing a stable power density of ~10 kW/kg_{anode}. Such electrodes are envisioned to be mass scalable with relatively simple and low-cost fabrication procedures, thereby providing a clear pathway toward commercialization.

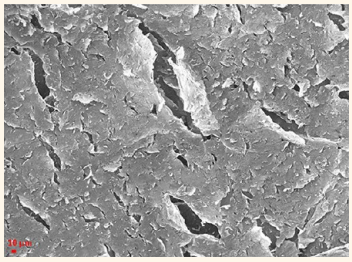

KEYWORDS: graphene · lithium-ion battery · high rower · rate capability · cycle life

Lithium-ion batteries have become integral to modern day portable electronic devices such as laptops and cellular phones. Moreover, with the advent of interest in electric vehicles (EV) and plug-in hybrid electric vehicles (HEV), the desire to develop lithium-ion batteries capable of incorporation in EVs and HEVs has risen significantly. Although lithium-ion batteries are shown to provide very high energy densities, they suffer from a critical drawback in that they are unable to provide high-power densities, which is quintessential for the aforementioned applications.[1] Thus there has been a major thrust in developing next generation lithium-ion batteries that are capable of providing both high-power and high-energy densities. A lithium-ion battery provides capacities through lithium intercalation with an active electrode material, and therefore, its high-rate performance is largely governed by Li^+ diffusivity and electron conductivity.[2,3] Some approaches in realizing high-rate capability have included incorporation of nanostructured anodes and cathodes that provide shorter Li^+ diffusion distances and using dopants for efficient electron transport.[4−7] However, stable performance over thousands of cycles of operation at charge/discharge rates (*C* rates) above 10 C has remained elusive. Moreover, mass scalability of nanostructured electrodes is challenging, and it is not clear whether such electrodes can be engineered to provide sufficient active electrode mass to build a viable battery.

Graphene, a single-carbon-atom thick two-dimensional sheet of sp^2-bonded carbon atoms has high electrical conductivity, large specific surface area, and mechanical robustness and is therefore a promising material for Li-ion battery anodes.[8−11] In fact, superior electrical conductivity of graphene nanosheets is often incorporated to improve the overall conductivity of anodes, as demonstrated by Cao *et al.*, whereby graphene provided a conductive network in TiO_2 anodes for efficient electron transfer kinetics at elevated charge/discharge rates as high as ~10 C.[12] In other studies, graphene-based composite anodes such as SnO_2−graphene and Fe_3O_4−graphene have also been successfully engineered where the presence of graphene not only improves the electron conductivity of the anodes but also prevents agglomeration of the nanoparticles and buffers the associated volume changes.[13−15]

Yoo *et al.* first tested pristine graphene nanosheet anodes in Li-ion batteries and demonstrated specific capacities of ~540 mAh/g.[16] Later, Fahlman and his group

* Address correspondence to koratn@rpi.edu.

Received for review May 17, 2012 and accepted August 10, 2012.

Published online August 11, 2012
10.1021/nn303145j

studied the performance of graphene nanoribbons.[17] Although they obtained an extremely high first cycle discharge capacity, the Coulombic efficiency was poor. In fact, both graphene nanosheets and nanoribbons did not display the impressive cycle stability of graphite. One possible reason for this could be the use of nonconducting polymer binders in sample preparation. This was later confirmed as one of the primary causes when Abouimrane *et al.* demonstrated improved cycling ability with a binder-free graphene electrode prepared *via* hydrazine-based reduction of free-standing graphene oxide paper.[18] The above studies with graphene anodes[16−18] were performed at charge/discharge rates (*C* rates) below 1 C.

It should be noted that achieving high capacities at elevated *C* rates is particularly challenging since the time available for lithium ions to diffuse through the anode and intercalate is now significantly shorter. As a result, only a partial lithiation is achieved, if at all, and the capacities are often very low. Another limitation with ultrahigh charge/discharge rates is the electron transfer mechanism. The electron conductivity of the anode material directly influences the charge transfer mechanism and thus largely governs the achievable *C* rates. Finally, a high surface area is desirable for operating at high rates since it is of prime importance that the lithium ions have sufficient active sites for intercalation to make up for the diffusivity constraints. In a recent breakthrough, high-rate capabilities were successfully achieved in N-doped and B-doped graphene with carbon black nanoparticles as conductive additives.[19] Zhao *et al.* have also demonstrated the role of nanopores as a means to achieve high-rate capabilities in pristine graphene, capable of delivering a maximum reversible capacity of ~178 mAh/g at a charge/discharge rate of ~5.4 C.[20]

Here we describe the photothermal reduction of free-standing graphene oxide paper to obtain graphene anodes with a unique "open-pore" structure. The energy from a camera flash or laser causes instantaneous and extensive heating of graphene oxide and induces a deoxygenation reaction.[10,21] We show that this rapid outgassing creates microscale pores, cracks, and voids in graphene paper, which enhances lithium intercalation kinetics at ultrafast charge/discharge rates. We attribute this to better ion diffusivity, greater access to the underlying graphene sheets through the micropores, and improved electrolyte wetting of the electrode. At a *C* rate of 5 C, we report a stable capacity of ~370 mAh/g, which is the highest capacity reported at 5 C for a pure carbon anode (without any additives) in a Li-ion cell. The capacity drops with increasing *C* rate, but the electrode is still capable of delivering an impressive ~156 mAh/g at 40 C and ~100 mAh/g at 100 C. Once again, these are by far the highest capacities reported so far for pure carbon-based anodes (without additives) at 40 and 100 C and are an order of magnitude higher than conventional graphitic anodes. Most importantly, these capacities were highly stable and could be maintained for over a thousand cycles of continuous high-rate charge/discharge. While laser-scribed graphene has recently been demonstrated in an electrochemical capacitor,[10] to our knowledge, this is the first demonstration of photoreduced graphene electrodes in lithium-ion batteries.

RESULTS

Fabrication and Characterization of Photothermally Reduced Graphene. Two procedures were adopted for fabricating photothermally reduced free-standing graphene paper, as shown schematically in Figure 1. First a Synrad Firestar T80 CO_2 laser cutting machine with a maximum power of 80 W, wavelength of 9.3 μm, and laser spot size of ~0.004 in. (*i.e.*, ~100 μm) was incorporated for reduction of graphene oxide. A raster pattern with a line spacing of 100 μm, which was equivalent to the laser spot size, was used. At any lesser line spacing, the graphene oxide paper disintegrated. The laser was operated at the lowest power setting of ~4.8 W, and in a single scan, a ~50 mm diameter graphene oxide paper was converted into laser-reduced graphene paper, as depicted schematically in Figure 1a. In the second approach, the photoflash in a simple digital camera (Samsung ES 15) was focused on the graphene oxide paper for reduction (Figure 1b). Distance between the flash and graphene oxide paper was maintained at ~1 cm, and multiple flashes were carried out to obtain a uniform reduction of graphene oxide. Both of the above processes yielded similar graphene structures and displayed similar performances as lithium-ion battery anodes as will be discussed later in this article. A photograph of flash-reduced graphene paper is shown in Figure 1c. The graphene paper is structurally robust and flexible and also very easy to handle and manipulate, as indicated in Figure 1c.

Scanning electron microscope (SEM) images obtained from a Carl Zeiss Supra 55 SEM system showed wide cracks and pores in photothermally reduced graphene as compared to graphene oxide (see SEM image in Figure 1d). Top view SEM image of flash-reduced graphene is included in Figure 2a, while a similar SEM image of laser-reduced graphene can be found in the Supporting Information (Figure S1). Deep cracks and pores that are several tens of micrometers in size are observed; such features are visibly absent in hydrazine-reduced graphene (Figure 2c). The underlying stacks of graphene sheets were clearly visible through these pores and cracks, which suggests better access for the electrolyte into the entire graphene structure and hence better lithium-ion transport and intercalation mechanisms. Moreover, both laser and flash reduction of graphene oxide provided a highly expanded structure (film cross section is shown in

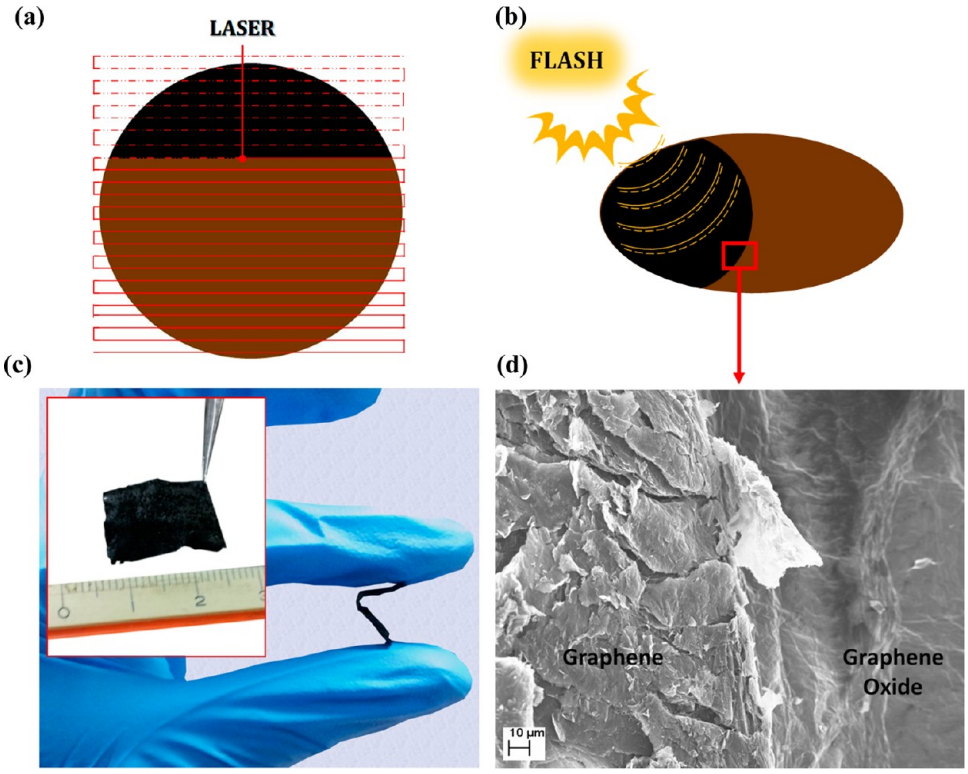

Figure 1. Photothermal reduction of graphene oxide. (a) Schematic showing the laser reduction system with the raster scan path. (b) Schematic showing the flash reduction of graphene oxide whereby a flash from a digital camera reduces graphene oxide. (c) Photograph of the flash-reduced graphene, displaying its structural integrity, and (d) scanning electron microscopy (SEM) image showing the two characteristic regions of flash-reduced graphene and graphene oxide. For this, a part of the graphene oxide sample was intentionally shielded from the photoflash in order to illustrate the contrast in porosity between the two regions.

Figure 2b) while surprisingly maintaining its integrity and robustness. The original thickness of the graphene oxide paper was ~10−20 μm, which expands to ~100 μm after the photoreduction. This expanded cross section showed large gaps between adjacent sheets of graphene. Therefore, the electrolyte can penetrate deep into the graphene anode not only *via* the pores and cracks on the film surface (Figure 2a) but also along the in-plane direction through the large continuous channels (Figure 2b) that are formed between the expanded graphene sheets. This could play an important role in facilitating lithium-ion diffusion and intercalation, particularly at high charge/discharge rates.

The extensive cracking/expansion of the graphene oxide film can be explained based on the instantaneous deoxygenation[10,21] of graphene oxide due to irradiation from laser or camera flashes over very short periods of time. The pressure generated by the rapid release and escape of oxygen is the principle cause behind the occurrences of such micropores, cracks, and voids in the film. This explanation is further validated by the fact that, when a chemically reduced (hydrazine-reduced) graphene paper (Figure 2c) is exposed to a similar laser scan, these micropores and cracks are not observed (Figure 2d). This demonstrates that rapid release of oxygen during the photoreduction process is instrumental in creating the expanded, open-pore structures shown in Figure 2a,b. While the photothermal reduction of graphene oxide has been demonstrated before,[10,11,21] our main focus in this article is to investigate how the open-pore structure of photothermally reduced graphene facilitates ultrafast intercalation kinetics in Li-ion battery anodes.

X-ray photoelectron spectroscopy (XPS) was used to study the surface chemistry of the photoreduced graphene samples. The results (Figure 3a−c) confirm that the majority of oxygen moieties are expelled as a result of the rapid photothermal heating of the samples. Photothermal treatment effectively reduces graphene oxide and drastically reduces the oxygen content as evidenced by the dominant C−C sp^2 peak[22] at 284.6 eV for the laser and flash-reduced samples. On the basis of the intensities of the C1s and O1s peaks, we estimate that the carbon to oxygen ratio is ~2 for graphene oxide paper, which increases to ~10.1:1 (9.9% oxygen) for the laser-reduced graphene and ~15.6:1 (6.4% oxygen) for the photoflash-reduced graphene. This indicates a highly effective reduction of graphene oxide by the photothermal method. Presence of oxygen-containing functional groups has been shown to promote irreversible capacities in graphene-based electrodes,[23] and hence, a lower oxygen

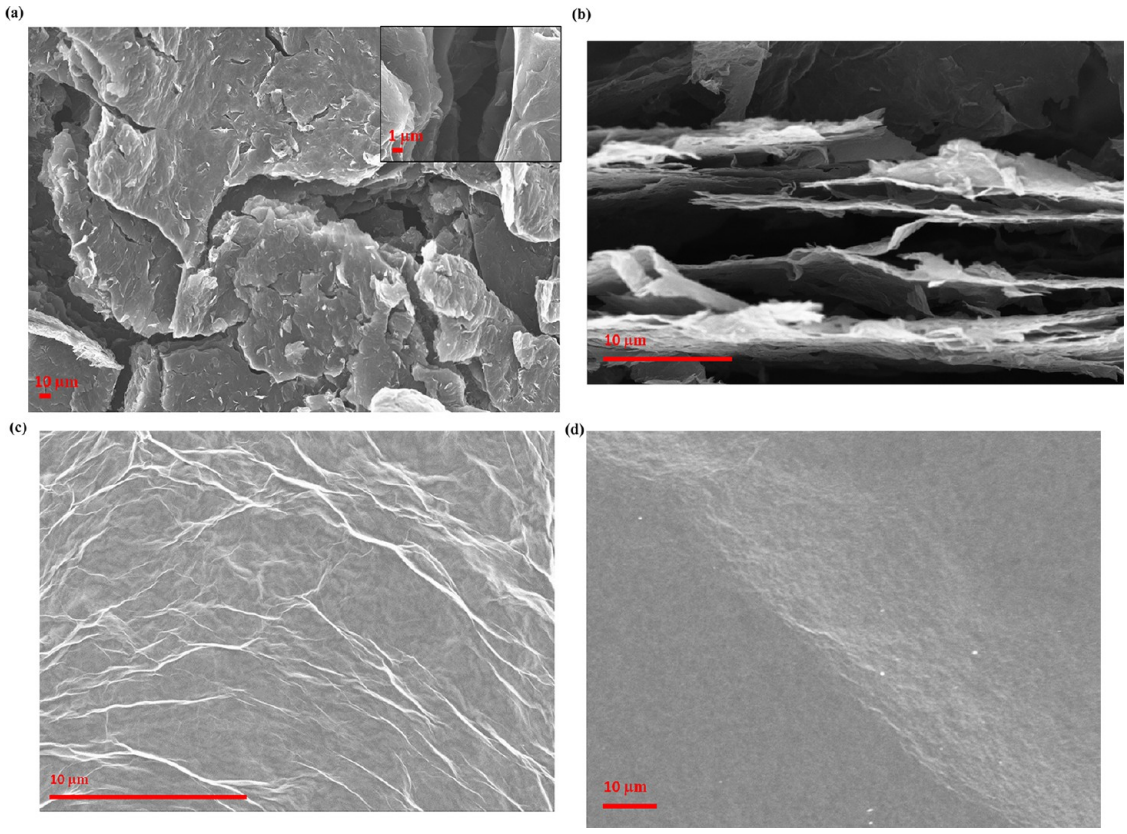

Figure 2. SEM characterization of photothermally reduced and hydrazine-reduced graphene oxide. (a) Top view image of flash-reduced graphene paper. The inset is a magnified image of a micrometer-scale crack that clearly shows underlying sheets of graphene exposed. (b) Cross-sectional image of laser-reduced graphene paper showing the expanded structure that enables greater access for lithium ions to active intercalation sites. The pores allow better flow of electrolyte into these voids and enable faster lithium-ion transport pathways. (c) Top view of hydrazine-reduced free-standing graphene paper clearly showing the absence of cracks and pores. (d) Laser scanning of graphene paper already reduced with hydrazine does not create pores or cracks, confirming that the wide cracks and pores observed in photothermally reduced graphene are caused by rapid deoxygenation reactions.

concentration is desirable for improved reversible capacities and high Coulombic efficiencies. The low oxygen content in photothermally reduced graphene is reflected in their Coulombic efficiencies as both laser and flash reduction facilitated early cycling Coulombic efficiencies in excess of 90%, while at a later cycling stage (>100 cycles), the Coulombic efficiencies were as high as 98 and 99% for laser-reduced and flash-reduced graphene, respectively (Supporting Information Figure S2).

The measured sheet resistances of the various samples are summarized in the Supporting Information Figure S3. The graphene oxide paper is electrically insulating, while the chemically (*i.e.*, hydrazine) reduced graphene showed the lowest resistivity. Photoflashed graphene and laser-reduced graphene show resistance values that are significantly higher than chemically reduced graphene. Therefore, purely from an electrical conductivity point of view, chemically reduced graphene shows the best results; however, it lacks the expanded pore structure of its photothermally reduced counterpart. Brunauer–Emmett–Teller (BET) specific surface area of the graphene electrodes was also measured with N_2 adsorption/desorption using a Quantachrome Autosorb-1 surface area and pore size analyzer. Typical specific surface area of the graphene electrodes was found to be in the 200–300 m^2/g range (Supporting Information, Figure S4).

Photothermally Reduced Graphene Anodes in Lithium-Ion Batteries. The graphene electrodes were assembled against Li foil in a two-electrode coin cell (2032) and cycled between 0.03 and 3 V at various charge/discharge rates (*C* rates). Figure 4a shows the typical measured voltage profile characteristics of photothermally reduced graphene anodes at *C* rates of 1 C (current density of ~0.372 A/g), 5 C (~1.86 A/g), and 40 C (~14.8 A/g). A *C* rate of *n* C means that the battery charges or discharges in 1/*n* hours. The voltage profiles in Figure 4a confirm the intercalation of the Li^+ ions into the electrode structure. The onset of intercalation is characterized by a reduction in the discharge slope; even at 40 C, such an intercalation stage is clearly visible at a little above ~500 mV, where the voltage drop becomes less steep.

At 1 C, photothermally reduced graphene provides a stable discharge capacity of ~545 mAh/g. Although

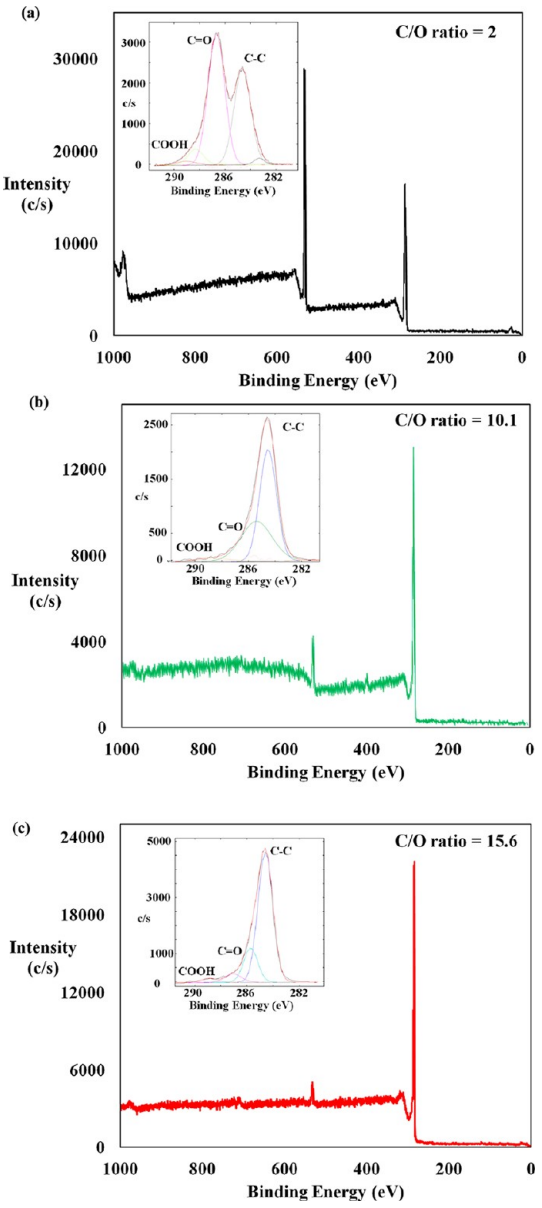

Figure 3. X-ray photoelectron spectroscopy (XPS) survey scans; inset plots show the details of the C1s peak. (a) Pristine graphene oxide, indicating a C/O ratio of ~2:1. (b) Laser reduction of graphene oxide shows improved deoxygenation with a C/O ratio of ~10.1:1. (c) Flash reduction of graphene oxide demonstrates excellent reduction through rapid deoxygenation induced by the flash. The C/O ratio of flash-reduced graphene is as high as ~15.6:1.

the theoretical capacity of carbon-based anodes is 372 mAh/g, higher capacities have often been reported in graphene-based anodes. The phenomenon has been attributed to different factors such as intercalation of Li ions on both sides of graphene sheets (corresponding to Li_2C_6)[24,25] and an increased *d* spacing, depending upon the number of stacked layers in graphene sheets.[16] The photothermally reduced graphene electrode's response at 1 C is therefore consistent with the literature. However, the electrode's performance at high *C* rates (*e.g.*, 5 C) is noteworthy. Typically, lithium-ion batteries operate at *C* rates of <1 C (1 C = charge/discharge time of 60 min), and 5 C (charge/discharge time of ~12 min) is considered a high-rate operating condition. The short discharge times at 5 C did not, however, impede the intercalation process as the cells still measured discharge capacities as high as ~370 and ~335 mAh/g_{anode} for flash-reduced and laser-reduced graphene, respectively. The ideal or theoretical capacity[26−28] of carbon anodes is ~372 mAh/g based on the formation of LiC_6. Such stable and near-theoretical capacities of carbon-based anodes have previously been observed only at much lower *C* rates (<1 C).[26,27] At 5 C, the cells could deliver power densities of ~1.2 kW/kg_{anode} and energy densities of ~244.5 and ~215 Wh/kg_{anode} for flash-reduced and laser-reduced graphene, respectively. Particularly noteworthy is the electrode response at an ultrafast *C* rate of 40 C (*i.e.*, charge/discharge in ~1.5 min). Even at 40 C, photothermally reduced graphene anodes are capable of delivering capacities as high as ~156 mAh/g_{anode}, as indicated in Figure 4a.

In order to obtain a clearer understanding of the extent of improvement, control tests were carried out with (a) conventional activated carbon electrode, (b) hydrazine-reduced graphene paper, and (c) hydrazine-reduced graphene paper that was subsequently laser scanned. These samples serve as appropriate controls for high-rate performance characterization. All of the cells, along with laser-reduced and flash-reduced graphene paper, were cycled at *C* rates of 5 C (*i.e.*, current density of ~1.86 A/g), 40 C (~14.8 A/g), 100 C (~37.2 A/g), 120 C (~44.6 A/g), and 150 C (~55.8 A/g) and then brought back to 5 C in the reverse order. The complete performance characteristic is shown in Figure 4b. The cells were run for 10 cycles at each of the *C* rates. Such stepped-rate studies enable a better understanding of the anode performance and, more importantly, provide information on the repeatability of the electrode performance. At a *C* rate of 5 C, hydrazine-reduced graphene paper provided average discharge capacity of ~55 mAh/g_{anode} while activated carbon control provides average discharge capacity of ~105 mAh/g_{anode}. These values are over 3−6-fold lower than the capacity of flash- and laser-reduced graphene at 5 C. Moreover, a large degradation in repeatability was observed for hydrazine-reduced graphene anodes as they could deliver only ~60% of its original capacity when it was cycled through various *C* rates and brought back to 5 C. Activated carbon also retained only ~88% of its original capacity. On the other hand, flash-reduced and laser-reduced graphene both exhibited excellent repeatability, providing ~95 and ~99.7% of its original capacity at 5 C after successive cycling (Figure 4b). As expected, the high-rate capability (at 40, 100, 120, and 150 C) of both activated carbon and hydrazine-reduced graphene was extremely poor. By contrast in the 40−150 C range, laser-

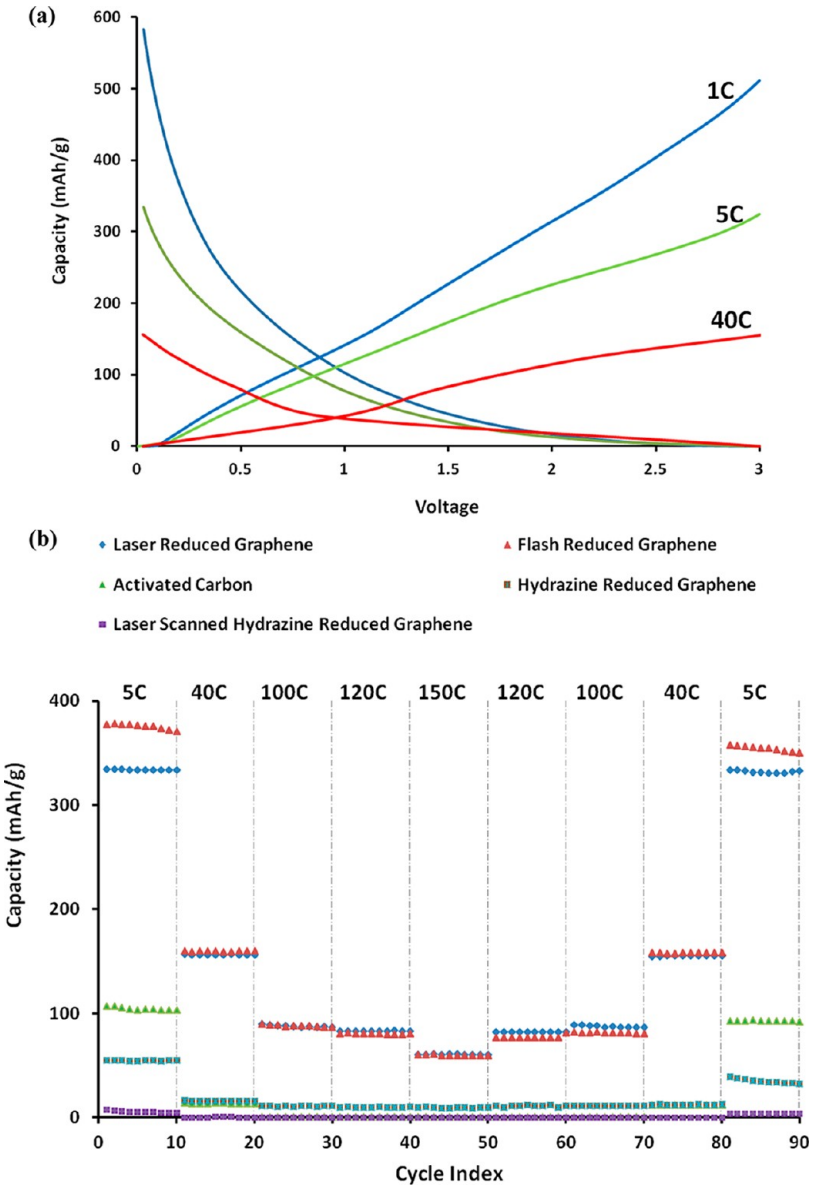

Figure 4. Performance of photothermally reduced graphene anodes in Li-ion cells. (a) Voltage profile of a laser-reduced graphene anode is shown at different *C* rates. (b) Performance of laser- and flash-reduced graphene anodes at various *C* rates, compared to the performance of control samples of activated carbon, hydrazine-reduced graphene, and laser-scanned hydrazine-reduced graphene. The cells were operated for 10 cycles each at different *C* rates from 5 to 150 C and were then brought back to 5 C in the reverse sequence. Photothermally reduced graphene not only shows order of magnitude higher capacities than control samples but also displays exceptional repeatability.

and flash-reduced graphene showed order of magnitude higher capacities as compared to the control samples.

To further study the long-term stability of the electrode, photoflash-reduced graphene anodes were tested at *C* rates of 20, 40, 120, and 150 C for over 1000 charge/discharge cycles. Capacity retentions of flash-reduced graphene anodes at 20 and 40 C were as high as ~98 and ~102.5% of the first cycle discharge capacity over 1000 charge/discharge cycles (Figure 5a). At 120 C, the capacity retention was ~94% over 1500 cycles, while at 150 C (charge/discharge in only ~24 s), the capacity retention was ~97% and the anodes could still deliver stable reversible capacities of ~61 mAh/$g_{electrode}$ over as many as 6000 charge/discharge cycles (Figure 5a). Such exceptional stability for graphene-based anodes is quite striking and has not been demonstrated before, especially over such a wide range of charge/discharge rates. This indicates that, in spite of its exfoliated and open structure and in spite of repeated Li^+ insertion and extraction at high rates, the photothermally reduced graphene electrode is still able to retain its structural integrity.

Further, when discussing high-rate applications, it is instructive to analyze the performance of anodes in terms of the Ragone plot. Figure 5b shows the

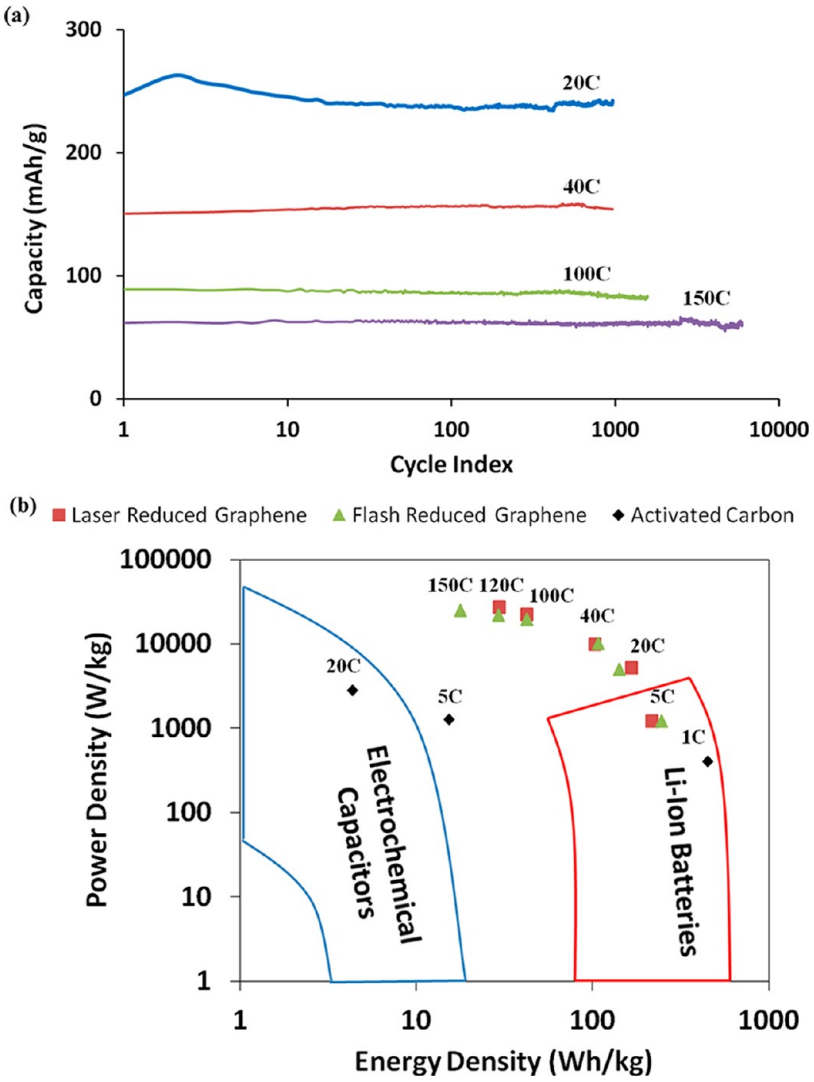

Figure 5. Long-term stability of photothermally reduced graphene anodes and Ragone plot. (a) Capacity *versus* cycle index plot for flash-reduced graphene showing highly stable performance. The cell was operated for ~1000 cycles at 20 and 40 C each, for ~1500 cycles at 120 C, and for ~6000 cycles at 150 C. (b) Ragone plot showing the energy density and power density of photothermally reduced graphene. For comparison, activated carbon control has also been plotted. Although activated carbon lies well within the lithium-ion battery region for lower *C* rates (1 C), its performance drastically reduces at higher power rates. Photothermally reduced graphenes on the other hand exhibit a smooth transition beyond the lithium-ion batteries region, thereby providing significantly higher energy and power densities. [The region for capacitors has been obtained from refs 7 and 10, while the region for lithium-ion batteries has been adopted from ref 29.]

performance of flash-reduced and laser-reduced graphene anodes in terms of its energy and power densities when compared with traditional carbon-based electrodes[7,10,29] for lithium-ion batteries and electrochemical capacitors. The performance of activated carbon, especially at high current densities, has also been plotted to provide a clearer comparison. At high current densities, the conventional activated carbon electrode rapidly loses energy density and behaves much like a conventional capacitor (*i.e.*, exhibits only surface-based reactions). On the other hand, flash- and laser-reduced graphene smoothly extends beyond the Li-ion batteries region, without transitioning to a rapid loss in energy density. More importantly, the cycle ability and repeatability of these anodes further suggest that these anodes are capable of switching back and forth between high-power and high-energy density applications when required by the system. From a practical perspective, this implies a wide range of operating conditions for various applications and especially so for electric vehicles, which have high-power demands during start-up and acceleration.

So far, we have focused only on photothermally reduced graphene electrodes. However, simple thermal reduction can also be used to reduce graphene oxide paper. In this method, the graphene oxide paper is injected into a chamber that is preheated to ~700 °C in an inert atmosphere to induce deoxygenation. This method also results in a free-standing, binder-free

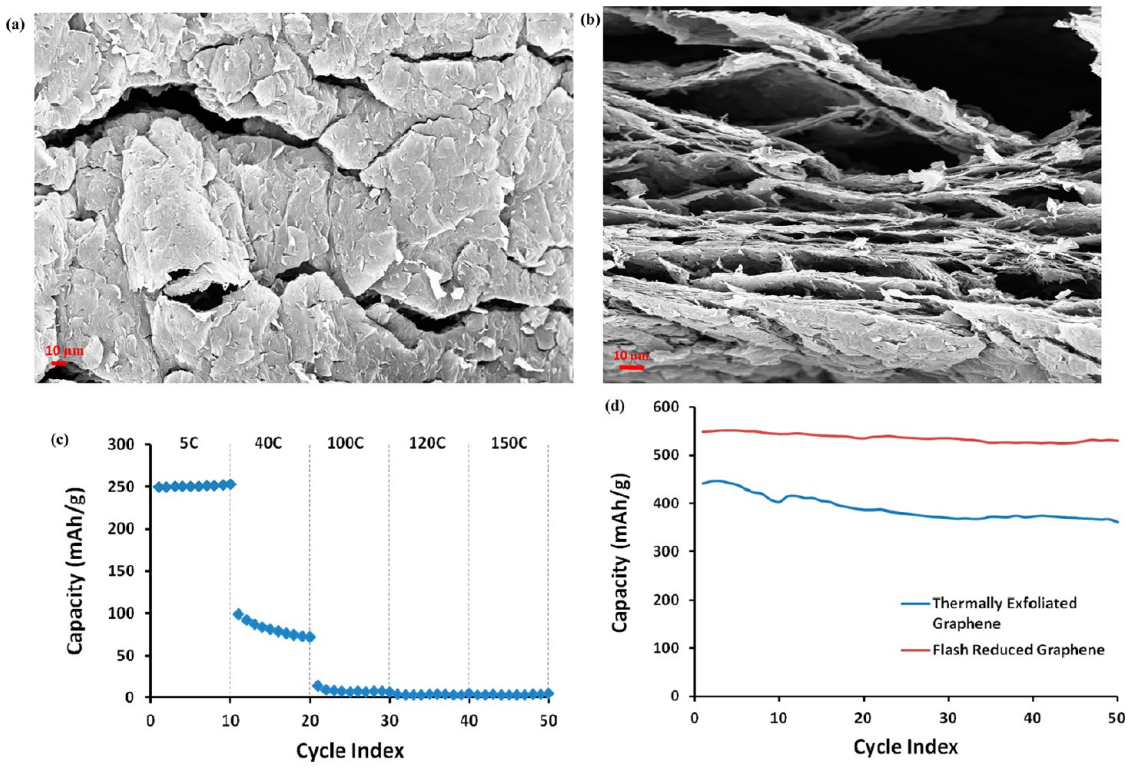

Figure 6. Thermally reduced free-standing graphene paper. (a) Top view and (b) cross-sectional SEM images of thermally reduced graphene paper show fewer cracks, pores, and intersheet voids as compared to photothermally reduced graphene. (c) Thermally reduced graphene shows a very significant drop in capacity with increasing charge/discharge rates. At 100 C, the electrode fails to provide any significant capacity. (d) Performance of thermally reduced graphene as compared to flash-reduced graphene at a low rate of 1 C. Thermally reduced graphene demonstrates less stability, showing an appreciable drop over just 50 charge/discharge cycles and retaining ~81.8% of the initial discharge capacity, while flash-reduced graphene retains as much as ~98.5% of the initial capacity.

graphene paper (Figure 6a,b) similar to the photothermal method. We tested such thermally reduced graphene paper as lithium-ion battery anodes and compared the results with photothermally reduced samples. Thermally reduced graphene provided a discharge capacity of ~250 mAh/g at a charge/discharge rate of 5 C (Figure 6c). However, the rate capability of thermally reduced graphene is considerably limited as compared to photothermally reduced graphene oxide. At 40 C, its capacity appears to drop significantly with cycling, while at higher rates of 100, 120, and 150 C, thermally reduced graphene fails to deliver appreciable capacities (Figure 6c). In photothermal reduction energy bursts over a very short time period from a camera flash or laser cause instantaneous and localized heating of graphene oxide, which induces a deoxygenation reaction.[10] The resulting outgassing generates local mini-explosions, leaving the surface pockmarked with microscale pores, cracks, and voids. By contrast, thermal reduction involves lower heating rates and is therefore not an instantaneous reduction process. As a consequence, thermal exfoliation provides more time for oxygen to diffuse out through the structure without opening up the tightly stacked graphene oxide structure. As a result, the presence of wide cracks and open pores is significantly reduced for thermally reduced graphene as compared to its photothermally reduced counterpart, as is evident from the SEM images shown in Figure 6a,b and Figure 2a,b. This is further confirmed by N_2 adsorption/desorption testing (using a Quantachrome Autosorb-1 pore size analyzer), which gave an average pore diameter of ~25 nm (Supporting Information Figure S4) for thermally reduced graphene. This is significantly lower than the average pore diameter of flash- and laser-reduced graphene, which was measured as high as 85.1 and 67.6 nm, respectively (Supporting Information Figure S4). The stability of thermally reduced graphene was also found to be lower than photothermally reduced graphene, as is evident in the decay in capacity at 1 C (see Figure 6d). At lower rates, such as 1 C, the intercalation is more and hence volume expansion becomes more evident. If the individual graphene sheets are not anchored well, volume expansion may potentially lead to a loss of electrical contact and, hence, a drop in performance. Furthermore, thermal reduction at 700 °C is not highly effective as determined from BET surface area measurements and C/O ratios from XPS. The surface area measured by BET was about ~152 m^2/g for thermally reduced graphene paper at 700 °C (Supporting Information Figure S4) as opposed to literature values of

600−900 m^2/g for thermally reduced graphite oxide at ~1050 °C.[30] Further from literature, the C/O ratio of thermally reduced graphite oxide at ~700 °C is around 6.4, which is significantly lower than the C/O ratio of ~13.2 for samples thermally reduced at ~1050 °C and that obtained for photothermally reduced graphene.[31] The lower C/O ratio thus contributes to higher irreversible capacities and hence lower Coulombic efficiencies. Note that it was not possible to increase the reduction temperature beyond ~750 °C while maintaining the structural integrity of the graphene oxide paper. Attempts to reduce the graphene oxide paper above ~750 °C resulted in the graphene oxide paper crumbling into a powder form. As a result of the aforementioned factors, thermally reduced free-standing graphene paper cannot match the rate capabilities, achievable capacities, and cycling stability of photothermally reduced graphene.

DISCUSSION

Photothermal reduction of free-standing graphene oxide paper yields a unique structure of graphene, with clearly visible micrometer-sized pores, cracks, and intersheet voids. The wide pores and cracks expose the underlying sheets of graphene and also provide better electrolyte access to the interior of the electrode. The cracks and voids also play a significant role in enhancing lithium-ion transport. As the electrolyte seeps through the cracks and pores, there is an added pathway created for lithium ions to reach the inner core of the graphene paper. Rather than having to diffuse through the graphene planes, lithium ions now have direct access to more active area through electrolyte transport. This is critical in high-power applications where the diffusion time often ranges from a few seconds to a few minutes. Diffusion time (t) is commonly characterized by $t = L^2/D$, where L is the diffusion distance (or sample thickness) and D is the diffusion coefficient. Diffusion coefficient of lithium ions in photoreduced graphene was determined using cyclic voltammetry and Randles−Sevcik equation[32,33] (Supporting Information Figure S5) and was estimated to be ~1.18×10^{-8} cm^2/s. The cross-sectional thickness of photoreduced graphene (Figure 2b) is ~100 μm, which would imply a diffusion time of ~850 s (corresponding to a C rate of ~4.2 C). The fact that photothermally reduced graphene anodes provide high discharge capacities in excess of 150 $mAh/g_{electrode}$ at almost 10 times the limiting rate (40 C) is indicative of the important role the pores, cracks, and expanded cross-sectional structure plays in lithium-ion intercalation kinetics. Because the electrolyte penetrates deep into the interior of the porous photoreduced graphene structure, the required Li^+ diffusion distances are now drastically reduced, which enables significant capacity retention at ultrafast charge/discharge rates.

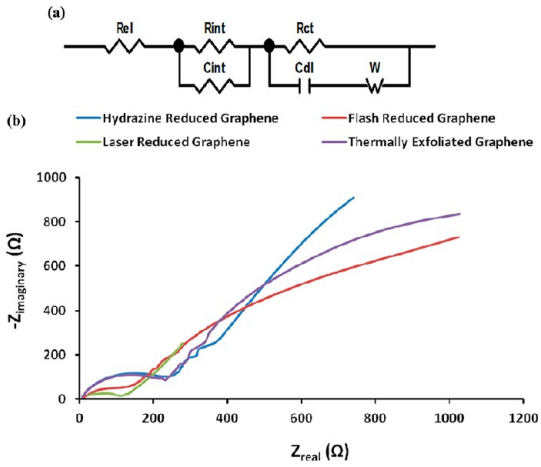

Figure 7. Electrochemical impedance spectroscopy (EIS) measurements. (a) Modified Randles equivalent circuit used to fit EIS data. (b) Nyquist plots of hydrazine-reduced, flash-reduced, laser-reduced, and thermally exfoliated free-standing graphene paper. EIS measurements were carried out between 10 kHz and 50 mHz after 1000 cycles at a charge/discharge rate of 40 C.

To further investigate the mechanisms contributing to superior rate capability of photothermally reduced graphene, electrochemical impedance spectroscopy (EIS) was carried out on hydrazine-reduced, flash-reduced, laser-reduced, and thermally reduced free-standing graphene paper using a Gamry Reference 3000 potentiostat. The frequency range was set between 10 kHz and 50 mHz, and EIS was carried out on each of the samples after 1000 charge/discharge cycles at a rate of 40 C after an equilibration time of 3 h. It is to be noted here that, although 1000 cycles is considered to be a very long cycle life, in this case, it was critical to perform EIS analysis after extended cycling to better study the excellent cycle life of photothermally reduced graphene along with the mechanisms behind the high capacities obtained at rapid charge/discharge rates. The capacity fade at C rate of 40 C has already been shown to be negligible (Figure 5a) even after 1000 charge/discharge cycles. As shown in Figure 7a, a modified Randles equivalent circuit was incorporated to fit the data points.[34,35] In the circuit, R_{el} represents the electrolyte resistance, R_{int} and C_{int} are the resistance and capacitance at the electrode−electrolyte interface, respectively; R_{ct} and C_{dl} are the charge transfer resistance and double-layer capacitance, respectively, and finally, W is the Warburg diffusion impedance. The high-frequency region in an EIS corresponds to the interfacial resistance at the surface of the active electrode. A higher interfacial resistance is generally indicative of a thick solid electrolyte interface (SEI) layer.[36] The middle-frequency region is attributed to charge transfer resistance. Lower charge transfer and interfacial resistances would significantly assist application of higher charge/discharge rates. Finally, the low-frequency spike is associated with impedance

attributed to the diffusion of lithium ions through the graphene sheets. Figure 7b shows Nyquist plots of flash-reduced, laser-reduced, hydrazine-reduced, and thermally reduced free-standing graphene anodes. The charge transfer resistance of laser-reduced and flash-reduced graphene was ~48.1 and ~73.2 Ω, respectively. The charge transfer resistance of thermally reduced graphene paper was slightly higher at ~85 Ω. In the case of hydrazine-reduced graphene, the charge transfer resistance was considerably higher at ~130.4 Ω. Charge transfer resistance is inversely related to the exchange current density through the equation $i_0 = RT/nFR_{ct}$, where R is the universal gas constant, T is the absolute temperature, n is the number of electrons, and F is Faraday's constant. Thus, photothermally reduced graphene anodes exhibit significantly improved electrochemical activity compared to hydrazine-reduced graphene. Importantly, in spite of the expanded structure of photothermally reduced graphene, the individual graphene sheets still appear to be networked strongly as evidenced by their low charge transfer resistance which facilitates efficient electron transfer at elevated *C* rates.

Another interesting observation was that the interfacial resistance of hydrazine-reduced graphene was much higher at ~95.1 Ω compared to ~14.2 and ~14.1 Ω for flash- and laser-reduced graphene, respectively. The interfacial resistance for thermally reduced graphene was measured as ~29.6 Ω. Such high interfacial resistance as obtained with hydrazine-reduced graphene may potentially affect efficient diffusion and initiation of intercalation of lithium ions, especially at the high *C* rates, where the ions do not have sufficient diffusion times. Moreover, since absence of an open-pore structure in hydrazine-reduced graphene demands that the lithium-ion diffusion should be through the surface of the anode, a thick SEI or high interfacial resistance can significantly limit the rate capabilities. In the case of laser- and flash-reduced graphene, interfacial resistances are significantly low, allowing for quick diffusion through the surface, while at the same time, the pores provide additional electrolytic pathways which increase the electrode-to-electrolyte contact area and enable ions to intercalate with the underlying graphene sheets. Low charge transfer and interfacial resistances together with the presence of wide pores and cracks thus enable the high-rate capability of photothermally reduced graphene. In the case of thermally reduced graphene, these resistances are higher as a result of which, although such electrodes perform reasonably well at rates of up to ~5 C (~12 min to charge/discharge), the capacities fade rapidly with a further increase in the *C* rates.

CONCLUSION

In conclusion, we present a study of photothermally reduced graphene anodes for lithium-ion batteries, particularly for high-power applications. The unique pore structure of these anodes enables their operation over a wide range of charge/discharge rates and can be envisioned as a stepping stone toward commercialization of graphene-based electrodes for various applications, including automotives where high-rate capabilities would enable the industry to circumvent the need to integrate additional energy storage units such as capacitors to deal with surges in power demand. Moreover, since photothermally reduced graphene is a free-standing (*i.e.*, self-supporting) mechanically robust electrode, the incorporation of current collectors and/or binders is negated. The mass of the electrode could also be scaled up by increasing the graphene oxide film thickness prior to the photoreduction step. However, it should be noted that the volumetric energy density of the electrode will be reduced due to its expanded structure. In order to improve the volumetric energy density of such a porous structure, the intersheet voids may be filled with active materials such as silicon, tin, or aluminum, which could further contribute to improving the charge storage capacity of the electrode. Finally, these anodes demonstrate excellent cycle life and repeatability and can be fabricated *via* relatively simple, quick, and inexpensive methods.

MATERIALS AND METHODS

Graphene oxide (GO) dispersed in deionized water (ACS Materials, 10 mg/mL) was diluted to concentrations of 0.2 and 2 mg/mL. These solutions were sonicated in a Bransonic 1510MT ultrasonic cleaner for 1 h to ensure homogeneous dispersion and centrifuged in a Sorvall Legend XTR centrifuge (Thermo Fisher Scientific) at 6000 rpm for 30 min to ensure removal of heavier aggregates. GO papers[37] were prepared by vacuum filtration of 50 mL of the supernatant GO solution through a 0.2 μm pore size Whatman Anodisc filter (47 mm diameter) to prepare papers of ~10−20 μm thicknesses, which were then carefully peeled off the filter and stored in a desiccator until further use. Then, 50 mL of the supernatant GO solution was converted to graphene by chemical reduction.[38] Briefly, this method involves the addition of hydrazine (35 wt % in water, Sigma-Aldrich) to GO solution maintaining a weight ratio of 7:10 in the presence of 0.02 wt % ammonia solution (28% in water, Sigma-Aldrich). Graphene paper is prepared by vacuum filtration from this stable dispersion of chemically reduced graphene.

Activated carbon anodes were prepared using the slurry method as described in ref 17, whereby 80% of activated carbon was mixed with 10% polyvinylidene fluoride (PVDF) binder and 10% carbon black conductive additive. *N*-Methyl-2-pyrrolidone (NMP) was then added to the mixture, and the slurry was pasted onto copper foil current collectors. All materials were obtained from Sigma-Aldrich. The slurry was then dried overnight at 120 °C inside a vacuum furnace.

Flash- and laser-reduced graphene, hydrazine-reduced graphene, laser-scanned hydrazine-reduced graphene, and activated carbon films were all tested as anodes. For this, 2032 coin

cells were assembled inside a glovebox (MBraun Labstar) with oxygen and moisture content <5 ppm. Lithium foil was used as the counter electrode, and a Celgard 2340 polypropylene membrane was used as the separator. The electrolyte was 1 M $LiPF_6$ in 1:1 mixture of ethylene carbonate (EC) and diethyl carbonate (DEC). Both the flash-reduced and laser-reduced graphene anodes were tested at various charge/discharge rates between 1 and 150 C. An Arbin BT2000 battery testing equipment was used to run the charge/discharge cycles. Cyclic voltammetry was carried out using Gamry Instrument's potentiostat/galvanostat Reference 3000.

In order to prepare thermally reduced free-standing graphene paper, the as-prepared GO paper was placed in a 1 in. diameter quartz tube with an argon flow of 500 sccm at atmospheric pressure. The sample was then rapidly introduced into a Thermolyne 79300 tube furnace kept at 700 °C and held for ~45 s. The heating causes deoxygenation[30,31] of the GO sheets to produce a binder-free structurally stable graphene paper.

Conflict of Interest: The authors declare no competing financial interest.

Acknowledgment. N.K. acknowledges funding support from the USA National Science Foundation (Award 0969895) and the John A. Clark and Edward T. Crossan Chair Professorship from the Rensselaer Polytechnic Institute. We would also like to thank David Guglielmo for help with operating the laser cutting machine and Dr. Xiang Sun for helping with BET characterization.

Supporting Information Available: SEM images of laser-reduced graphene paper, Coulombic efficiencies of flash- and laser-reduced graphene, sheet resistance of laser-reduced, flash-reduced, hydrazine-reduced, and laser-treated hydrazine-reduced graphene, Brunauer–Emmett–Teller (BET) specific surface area- and pore size distribution analysis of flash-reduced, laser-reduced, and thermally reduced free-standing graphene paper and cyclic voltammetry of photothermally reduced graphene. This material is available free of charge *via* the Internet at http://pubs.acs.org.

REFERENCES AND NOTES

1. Tarascon, J.-M.; Armand, M. Issues and Challenges Facing Rechargeable Lithium Batteries. *Nature* **2001**, *414*, 359–367.
2. Kang, B.; Ceder, G. Battery Materials for Ultrafast Charging and Discharging. *Nature* **2009**, *458*, 190–193.
3. Herle, P. S.; Ellis, B.; Coombs, N.; Nazar, L. F. Nano-Network Electronic Conduction in Iron and Nickel Olivine Phosphates. *Nat. Mater.* **2004**, *3*, 147–152.
4. Chan, K. C.; Zhang, X. F.; Cui, Y. High Capacity Li Ion Battery Anodes Using Ge Nanowires. *Nano Lett.* **2008**, *8*, 307–309.
5. Krishnan, R.; Lu, T.-M.; Koratkar, N. Functionally Strain-Graded Nanoscoops for High Power Li-Ion Battery Anodes. *Nano Lett.* **2011**, *11*, 377–384.
6. Ghosh, P.; Mahanty, S.; Basu, R. N. Lanthanum-Doped $LiCoO_2$ Cathode with High Rate Capability. *Electrochim. Acta* **2009**, *54*, 1654–1661.
7. Simon, P.; Gogotsi, Y. Materials for Electrochemical Capacitors. *Nat. Mater.* **2008**, *7*, 845–854.
8. Park, S.; Ruoff, R. S. Chemical Methods for the Production of Graphenes. *Nat. Nanotechnol.* **2009**, *4*, 217–224.
9. Zhu, N.; Liu, W.; Xue, M.; Xie, Z.; Zhao, D.; Zhang, M.; Chen, J.; Cao, T. Graphene as a Conductive Additive To Enhance the High-Rate Capabilities of Electrospun $Li_4Ti_5O_{12}$ for Lithium-Ion Batteries. *Electrochim. Acta* **2010**, *55*, 5813–5818.
10. El-Kady, M. F.; Strong, V.; Dubin, S.; Kaner, R. B. Laser Scribing of High-Performance and Flexible Graphene-Based Electrochemical Capacitors. *Science* **2012**, *335*, 1326–1330.
11. Gao, W.; Singh, N.; Song, L.; Liu, Z.; Reddy, A. L. M.; Ci, L.; Vajtai, R.; Zhang, Q.; Wei, B.; Ajayan, P. M. Direct Laser Writing of Micro-Supercapacitors on Hydrated Graphite Oxide Films. *Nat. Nanotechnol.* **2011**, *6*, 496–500.
12. Cao, H.; Li, B.; Zhang, J.; Lian, F.; Kong, X.; Qu, M. Synthesis and Superior Anode Performance of TiO_2@Reduced Graphene Oxide Nanocomposites for Lithium Ion Batteries. *J. Mater. Chem.* **2012**, *22*, 9759–9766.
13. Paek, S.-M.; Yoo, E. J.; Honma, I. Enhanced Cyclic Performance and Lithium Storage Capacity of SnO_2/Graphene Nanoporous Electrodes with Three-Dimensionally Delaminated Flexible Structure. *Nano Lett.* **2009**, *9*, 72–75.
14. Lian, P.; Zhu, X.; Xiang, H.; Li, Z.; Yang, W.; Wang, H. Enhanced Cycling Performance of Fe_3O_4-Graphene Nanocomposite as an Anode Material for Lithium-Ion Batteries. *Electrochim. Acta* **2010**, *56*, 834–840.
15. Wang, J.-Z.; Zhong, C.; Wexler, D.; Idris, N. H.; Wang, Z.-X.; Chen, L.-Q.; Liu, H.-K. Graphene-Encapsulated Fe_3O_4 Nanoparticles with 3D Laminated Structure as Superior Anode in Lithium Ion Batteries. *Chem.—Eur. J.* **2011**, *17*, 661–667.
16. Yoo, E. J.; Kim, J.; Hosono, E.; Zhou, H.-S.; Kudo, T.; Honma, I. Large Reversible Li Storage of Graphene Nanosheet Families for Use in Rechargeable Lithium Ion Batteries. *Nano Lett.* **2008**, *8*, 2277–2282.
17. Bharadwaj, T.; Antic, A.; Pavan, B.; Barone, V.; Fahlman, B. D. Enhanced Electrochemical Lithium Storage by Graphene Nanoribbons. *J. Am. Chem. Soc.* **2010**, *132*, 12556–12558.
18. Abouimrane, A.; Compton, O. C.; Amine, K.; Nguyen, S. Non-annealed Graphene Paper as a Binder-Free Anode for Lithium-Ion Batteries. *J. Phys. Chem. C* **2010**, *114*, 12800–12804.
19. Wu, Z.-S.; Ren, W.; Xu, L.; Li, F.; Cheng, H.-M. Doped Graphene Sheets as Anode Materials with Superhigh Rate and Large Capacity for Lithium Ion Batteries. *ACS Nano* **2011**, *5*, 5463–5471.
20. Zhao, X.; Hayner, C. M.; Kung, M. C; Kung, H. H. Flexible Holy Graphene Paper Electrodes with Enhanced Rate Capability for Energy Storage Applications. *ACS Nano* **2011**, *5*, 8739–8749.
21. Cote, L. J.; Cruz-Silva, R.; Huang, J. Flash Reduction and Patterning of Graphite Oxide and Its Polymer Composite. *J. Am. Chem. Soc.* **2009**, *131*, 11027–11032.
22. Strong, V.; Dubin, S.; El-Kady, M. F.; Lech, A.; Wang, Y.; Weiller, B. H.; Kaner, R. B. Patterning and Electronic Tuning of Laser Scribed Graphene for Flexible All-Carbon Devices. *ACS Nano* **2012**, *6*, 1395–1403.
23. Zhou, G.; Wang, D.-W.; Li, F.; Zhang, L.; Li, N.; Wu, Z.-S.; Wen, L.; Lu, G. Q.; Cheng, H. M. Graphene-Wrapped Fe_3O_4 Anode Material with Improved Reversible Capacity and Cyclic Stability for Lithium Ion Batteries. *Chem. Mater.* **2010**, *22*, 5306–5313.
24. Wang, G.; Shen, X.; Yao, J.; Park, J. Graphene Nanosheets for Enhanced Lithium Storage in Lithium Ion Batteries. *Carbon* **2009**, *47*, 2049–2053.
25. Dahn, J. R.; Zheng, T.; Liu, Y.; Xue, J. S. Mechanisms for Lithium Insertion in Carbonaceous Materials. *Science* **1995**, *270*, 590–593.
26. Teki, R.; Datta, M. K.; Krishnan, R.; Parker, T. C.; Lu, T.-M.; Kumta, P. N.; Koratkar, N. Nanostructured Silicon Anodes for Lithium Ion Rechargeable Batteries. *Small* **2009**, *5*, 2236–2242.
27. Maranchi, J. P.; Hepp, A. F.; Evans, A. G.; Nuhfer, N. T.; Kumta, P. N. Interfacial Properties of the a-Si/Cu: Active–Inactive Thin-Film Anode System for Lithium-Ion Batteries. *J. Electrochem. Soc.* **2006**, *153*, A1246–A1253.
28. Zhang, H.-B.; Wang, J.-W.; Yan, Q.; Zheng, W.-G.; Chen, C.; Yu, Z.-Z. Vacuum-Assisted Synthesis of Graphene From Thermal Exfoliation and Reduction of Graphite Oxide. *J. Mater. Chem.* **2011**, *21*, 5392–5397.
29. Dubarry, M.; Truchot, C.; Cugnet, M.; Liaw, B. Y.; Gering, K.; Sazhin, S.; Jamison, D.; Michelbacher, C. Evaluation of Commercial Lithium-Ion Cells Based on Composite Positive Electrode for Plug-in Hybrid Electric Vehicle Applications. Part I: Initial Characterizations. *J. Power Sources* **2011**, *196*, 10328–10335.
30. Schniepp, H. C.; Li, J. L.; McAllister, M. J.; Sai, H.; Herrera-Alonso, M.; Adamson, D. H.; Prud'homme, R. K.; Car, R.; Saville, D. A.; Aksay, I. A. Functionalized Single Graphene Sheets Derived from Splitting Graphite Oxide. *J. Phys. Chem. B* **2006**, *110*, 8535–8539.

31. McAllister, M. J.; Li, J. L.; Adamson, D. H.; Schniepp, H. C.; Abdala, A. A.; Liu, J.; Herrera-Alonso, M.; Milius, D. L.; Car, R.; Prud'homme, R. K.; *et al.* Single Sheet Functionalized Graphene by Oxidation and Thermal Expansion of Graphite. *Chem. Mater.* **2007**, *19*, 4396–4404.
32. Hu, R.; Zeng, M.; Li, C. Y. V.; Zhu, M. Microstructure and Electrochemical Performance of Thin Film Anodes for Lithium Ion Batteries in Immiscible Al−Sn System. *J. Power Sources* **2009**, *188*, 268–273.
33. Mukherjee, R.; Krishnan, R.; Lu, T.-M.; Koratkar, N. Nanostructured Electrodes for High-Power Lithium Ion Batteries. *Nano Energy* **2012**, *1*, 518–533.
34. Yang, S.; Song, H.; Chen, X. Electrochemical Performance of Expanded Mesocarbon Microbeads as Anode Material for Lithium Ion Batteries. *Electrochem. Commun.* **2006**, *8*, 137–142.
35. Zhang, S. S.; Xu, K.; Jow, T. R. Electrochemical Impedance Study on the Low Temperature of Li-Ion Batteries. *Electrochim. Acta* **2004**, *49*, 1057–1061.
36. Guo, P.; Song, H.; Chen, X. Electrochemical Performance of Graphene Nanosheets as Anode Material for Lithium-Ion Batteries. *Electrochem. Commun.* **2009**, *11*, 1320–1324.
37. Dikin, D. A.; Stankovich, S.; Zimney, E. J.; Piner, R. D.; Dommett, G. H. B.; Evmenenko, G.; Nguyen, S. T.; Ruoff, R. S. Preparation and Characterization of Graphene Oxide Paper. *Nature* **2007**, *448*, 457–460.
38. Li, D.; Muller, M. B.; Gilje, S.; Kaner, R. B.; Wallace, G. G. Processable Aqueous Dispersions of Graphene Nanosheets. *Nat. Nanotechnol.* **2008**, *3*, 101–105.